ChemComm

COMMUNICATION

View Article Online
View Journal | View Issue

Cite this: *Chem. Commun.*, 2017, 53, 10054

Received 18th July 2017,
Accepted 14th August 2017

DOI: 10.1039/c7cc05552h

rsc.li/chemcomm

A highly stable polyoxometalate-based metal–organic framework with an ABW zeolite-like structure†

Xiao-Xin Li,‡[a] Feng-Cui Shen,‡[bc] Jiang Liu,[b] Shun-Li Li,[b] Long-Zhang Dong,[b] Qiang Fu,[a] Zhong-Min Su*[a] and Ya-Qian Lan*[b]

A novel polyoxometalate-based metal–organic framework (POMOF) with an ABW network, NENU-601, was synthesized *in situ*. To the best of our knowledge, this is the first POMOF with a zeolite-like structure, which was designed by regulating the length and angle of mixed ligands and rationally choosing suitable Polyoxometalates (POMs) as nodes.

Zeolites are a significant class of inorganic crystalline materials with wide applications like in petroleum refining, catalysis, ion-exchanging and so on[1–3] due to their remarkable chemical and thermal stability, which are necessarily built from MO_4 tetrahedra (M = Si, Al or P, *etc.*) and connected to four adjacent tetrahedra by vertex O atoms leading to 3D four-connected frameworks.[4–7] The only fly in the ointment is that zeolites can only adjust the ratio of Si : Al for functionalisation.[8] To break the bottleneck, researchers tried to utilize crystallographic theory to tunably synthesize more zeolite-like structures.[9] Metal–organic frameworks (MOFs), a class of materials constructed with metal ions or clusters as nodes and multi-functional organic ligands as linkers, have received much attention because of their high surface areas and tunable structures.[10–14] As for this point, nodes and linkers can be well-designed to get the expected structures, pore volumes, functions and properties.[15,16] One representative sub-family of MOFs is the group of zeolite-like MOFs (ZMOFs) that use tetrahedral-connected nodes and ligands corresponding to Si/Al–O tetrahedra and O atoms, respectively, combining the advantages of MOFs and the high stability of zeolites. In particular, a series of frameworks have been synthesised in recent decades by assembling Zn^{2+} or Co^{2+} ions and imidazolates, namely zeolitic imidazolate frameworks (ZIFs),[17–19] which have drawn extensive attention and research due to their zeolite-like structures (Scheme 1).

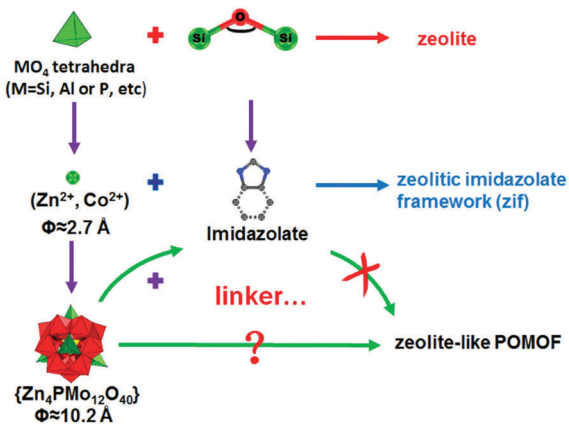

Scheme 1 Schematic representation of the design strategies for the construction of a zeolite, ZIF and ZPOMOF.

Compared to the synthesis of novel structures, the derived material applications are more concerning. Recently, a large number of MOFs have been applied as electrode materials for batteries to solve energy issues due to their porosity and large surface areas. However, the problem with using MOFs directly for electrode materials is that the poor redox ability of normal MOFs affects their reversible capacity, which greatly restricts their energy storage applications. POMs are a subset of inorganic clusters that contain various metal ions which reveal superior performances in redox reactions and favourable Lewis and Brønsted acidity, resulting in their application in various fields.[20–22] Therefore, more attention has been focused on introducing POM units to MOFs to construct POMOFs.[23] POMOFs can almost be divided into two types: one has loaded POMs as templates in the network of known MOFs and the other has fixed POMs in the framework of MOFs as nodes connected to ligands. To date, POMOFs have been synthesized and applied

[a] *Institute of Functional Material Chemistry, Department of Chemistry, National & Local United Engineering Lab for Power Battery, Northeast Normal University, Changchun 130024, Jilin, P. R. China. E-mail: zmsu@nenu.edu.cn*
[b] *School of Chemistry and Materials Science, Nanjing Normal University, Nanjing 210023, P. R. China. E-mail: yqlan@ninu.edu.cn*
[c] *School of Biological and Chemical Engineering, Anhui Polytechnic University, Wuhu, 241000, P. R. China*

† Electronic supplementary information (ESI) available. CCDC 1555051. For ESI and crystallographic data in CIF or other electronic format see DOI: 10.1039/c7cc05552h
‡ These authors contributed equally to this work.

to some fields like heterogeneous electro/photocatalysis, electroanalytical domains, proton conductivity and chemical separations.[23] This kind of framework has shown excellent development prospects because of its stable skeleton and high redox ability. But there is no report on the structure of zeolite-like POMOF (ZPOMOF) materials. Design strategies for the construction of ZPOMOFs are still under exploration and here are some feasible methods and difficulties:

(i) POMs are utilized as templates and synthesized inside the cages of ZMOFs. But the big volume of the POMs causes them to be hardly implanted in pores of the known ZMOFs;

(ii) POMs are used to replace metal ions or clusters as nodes in the network of the available MOFs. But there are few kinds of POM that possess suitable 4-connected nodes. Moreover, the size of the POMs is approximately five times larger than metal ions so it is not easy to choose suitable ligands to match POMs and form 3D frameworks.

The strategy of designing the structure in this work can be divided into three modules. The 4-connected POM node we chose is the ε-$\{Zn_4PMo_{12}O_{40}\}$ cluster. The imidazolate or triazole ligands provide a metal–Im–metal angle that has a similar value to the Si–O–Si angle in zeolites. Furthermore, the moderate length of the linker is also a critical parameter to choose when building ZPOMOFs. Based on the points above, through our topological calculation and design, we finally chose Hbzt as the ligand to provide the 145° metal–Im–metal angle and 1,4H_2bdc as the secondary bridging ligand (Fig. S1, ESI†). As expected, we successfully synthesized the first POMOF with an ABW zeolite-like topological structure (**NENU-601**). It shows high chemical and thermal stability which means that it can keep its crystalline integrity in aqueous solution in a range of pH values from 1 to 12 and keep its skeleton intact at 370 °C (Fig. S4, ESI†). We directly utilized **NENU-601** as an anode material for lithium-ion batteries (LIBs). This rigid structure showed its superior chemical and structural stability during the electrochemical process, and the ε-$\{Zn_4PMo_{12}O_{40}\}$ cluster units as SBUs showed favourable and reversible performances.

X-ray crystallography revealed that **NENU-601** crystallized in the orthorhombic space group *Ibam* with eight formula units ($Z = 8$) per unit cell (Table S1, ESI†). The asymmetric unit consists of the inorganic building unit of ε-$\{Zn_4PMo_{12}O_{40}\}$ and organic ligands including three deprotonated bzt^- units and one bdc^{2-} unit. The ε-$\{Zn_4PMo_{12}O_{40}\}$ cluster is a member of compounds based on the ε-Keggin $\{PMo_{12}O_{40}\}$ anion which has four capping Zn(II) ions. This inorganic building block has a tetrahedral configuration and Zn(II) ions in the vertex, providing the possibility of forming a 3D network. Each Zn(II) ion has a distorted tetrahedral geometry and the Zn(II)-bzt-Zn(II) angles vary from 133° to 137°, which is near to the 145° that we expected. The coordination modes of the Zn(II) ions can be divided into two distinct types. Three of them (Zn2, Zn3 and Zn4) are coordinated to three nitrogen atoms (N2, N1#1 and N4) belonging to the bzt^- ligands and the remaining one (Zn1) is coordinated to an oxygen atom (O1) from the carboxylate group of the bdc^{2-} ligands (Fig. 1a). The average Zn–N and Zn–O distances are 1.983 Å and 1.927 Å, respectively. In the topology analysis,

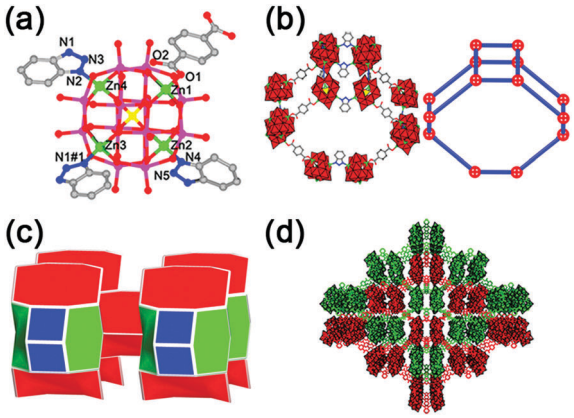

Fig. 1 Summary of the structure of **NENU-601**: (a) the coordination environments of the Zn(II) centers in **NENU-601**, all hydrogen atoms are omitted for clarity. Symmetry codes: #1 0.5 + x, 0.5 − y, z. (b) Representation of a single code in the ABW zeolite-like topology. (c) Tiling diagram of the ABW zeolite-like net. (d) Twofold interpenetrating 3D framework of **NENU-601**.

ε-$\{Zn_4PMo_{12}O_{40}\}$ is considered as 4-connected nodes and the mixed ligands of Hbzt and H_2bdc as 2-connected linkers that are simplified. It showed that **NENU-601** consists of 4-, 6- and 8-rings (Fig. S2, ESI†) according to the same point Schläfli symbol of $\{4^2.6^3.8\}$, which reveals that the topology of **NENU-601** is an ABW zeolite-like code (Fig. 1b).[24,25]

Meanwhile, we depict the tiling diagram of the ABW zeolite-like net in Fig. 1c. Interestingly, in this structure, the same two frameworks interlock, leading to an interpenetrated framework (Fig. 1d) with zeolite-like structures, which has rarely appeared before. To confirm the final formula, as we calculated, the TBA^+ ions are free in the channels to balance the charges even though they cannot be proven to exist through single-crystal X-ray diffraction.

We noted that many interesting pioneering studies on POMOFs have been reported using common azole ligands and carboxylate ligands.[26–28] Anne Dolbecq's group reported a 0D structure **ε(bim)$_4$** using benzimidazole (Hbim) as a single ligand (Fig. 2a).[29] The reason why it could not form a 3D framework is probably because the length of Hbim is not enough to connect two POM nodes because of their quite large steric hindrance. (The Keggin node is approximately four times the diameter of Zn^{2+}). Therefore, a linear ligand plays an important role in acting as a secondary ligand because its coordination mode is more favorable to form a 3D network and its linear shape can reduce the impact of steric hindrance from POMs. Then they tried to add another bidentate carboxylate ligand like 1,4-H_2bdc (6.995 Å) or 4,4′-biphenyldicarboxylic acid (H_2biphen, 11.280 Å) as a secondary bridging ligand to prompt the 0D molecule to form a 3D framework due to the fact that 1,4-H_2bdc can be employed to form a 3D POMOF in the diamondoid-structured **Z-POMOF1** (Fig. 2b).[26] In fact, the combination of Hbim and H_2biphen finally resulted in the 0D cluster **ε(bim)$_3$(biphen)$_{1/2}$** (Fig. 2c)[28] where each bim^- is just connected to one ε-$\{Zn_4PMo_{12}O_{40}\}$. Therefore, by comparing the above studies with **NENU-601** (Fig. 2d), we conclude that a linker with a reasonable length is necessary to construct ZPOMOFs.

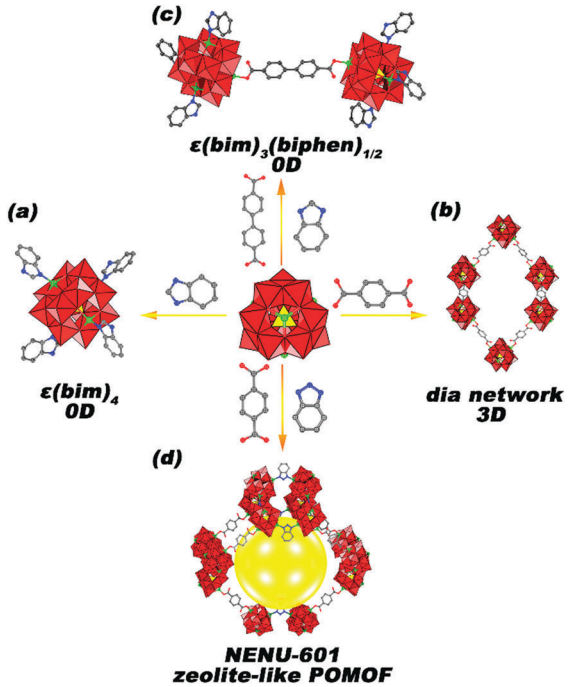

Fig. 2 Reported POMOFs constructed by common azole ligands and carboxylate ligands (a–c): ε-{$Zn_4PMo_{12}O_{40}$} linked with Hbim, H_2bdc and hybrid Hbim and H_2biphen leads to 0D **ε(bim)$_4$**, 3D **Z-POMOF1** in dia network and 0D **ε(bim)$_3$(biphen)$_{1/2}$**, correspondingly. (d) ε-{$Zn_4PMo_{12}O_{40}$} clusters linked with Hbzt and H_2bdc lead to 3D **NENU-601** with an ABW zeolite-like structure.

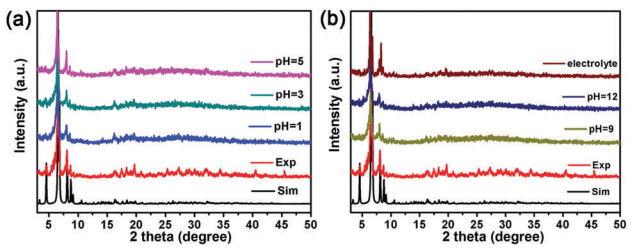

Fig. 3 PXRD patterns of **NENU-601**, with the as-synthesized sample immersed in electrolyte at room temperature for 12 h and in aqueous solution with different pH values for 24 h. "Sim" represents the simulated pattern and "Exp" represents the pattern of the as-synthesized sample.

The phase purity of rhombus crystalline **NENU-601** was determined by comparing experimental and simulated powder X-ray diffraction (PXRD) patterns (Fig. 3). **NENU-601** can be stable in air for more than 300 days, furthermore, the patterns obviously reveal that the crystalline integrity of **NENU-601** means that it can be kept in aqueous solution in different pH values (pH = 1, 3, 5, 9, 11 and 12, adjusted by HCl or NaOH) for 24 hours and in electrolyte for 12 hours, which indicates that **NENU-601** has excellent chemical stability. The stability in electrolyte shows the possibility of utilizing **NENU-601** as an electrode material and guarantees the cyclic stability of LIBs.

The highly stable structure lays the foundation for its application in LIBs. As we predicted, **NENU-601** revealed excellent electrochemical performance, indicated by electrochemical measurements

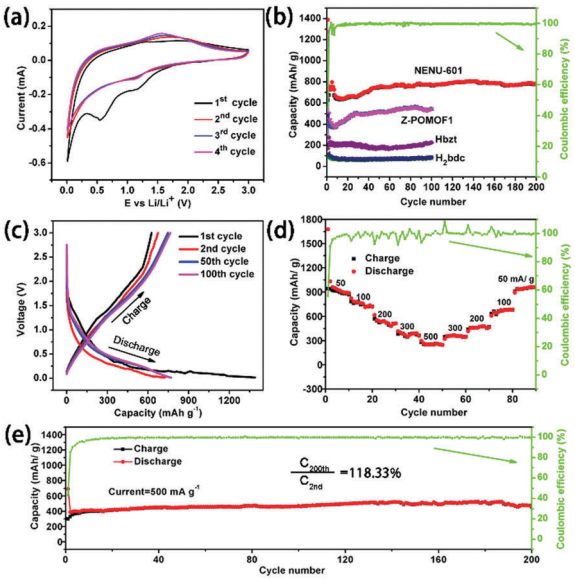

Fig. 4 Electrochemical performances of **NENU-601** anodes. The specific capacity was calculated based on the mass of the active material. (a) CV profiles of **NENU-601** at a scan rate of 0.2 mV s^{-1}. (b) Cycling performances of **NENU-601**, **Z-POMOF1**, 1,4-H_2bdc and Hbzt at a current density of 100 mA g^{-1} for each. (c) Charge/discharge profiles of **NENU-601** for different cycles constantly at 100 mA g^{-1}. (d) **NENU-601** cycled at various current densities. (e) Stability test of **NENU-601** for 200 cycles at 500 mA g^{-1}.

such as cyclic voltammetry (CV), as well as excellent charge–discharge voltage, cycling performance and rate performance. Fig. 4a shows the CV curves in the voltage range from 0.01 to 3.0 V (scan rate = 0.2 mV s^{-1}). The cathodic peak at 0.6 V in the first discharge was ascribed to the formation of a solid–electrolyte interphase (SEI) film. In the next two cycles, the reversibility of 1.1 V for the reductive peak and 1.5 V for the oxidative peak indicates an electrochemical process, which may be a consequence of the redox reaction of Zn and Mo.[30,31] It also demonstrates the good cycle stability for the superposition of the following curves in Fig. 4c. The cycling performance of **NENU-601** is shown in Fig. 4b with a current density of 100 mA g^{-1}. **NENU-601** obtains a discharge specific capacity at 1389.1 mA h g^{-1} in the 1st cycle and its first charge specific capacity can deliver 626.6 mA h g^{-1}, which results in an initial coulombic efficiency (CE) of over 45%. The initial irreversible capacity loss is principally because of the formation of the SEI film after the electrolyte decomposes. Along with the charge–discharge process, the pore activation of **NENU-601** causes the reversible capacity to be 780 mA h g^{-1} after 200 cycles as a result of its stable framework,[32,33] which is superior to that for previously reported porous materials (Table S4, ESI†). At the same time, we chose **Z-POMOF1** (Fig. S5, ESI†) for the comparison. **Z-POMOF1** achieves a capacity of 545 mA h g^{-1} under the same testing conditions after 100 cycles. In addition, pure Hbzt and H_2bdc ligands are also tested and achieve capacities of 216 mA h g^{-1} and 148 mA h g^{-1}, respectively. **NENU-601** has better lithium ion storage properties than **Z-POMOF1** because it benefits from lower impedance (Fig. S6, ESI†) and the contribution of N-containing ligands.

NENU-601 also has a good rate performance at various current densities from 50 to 500 mA g^{-1} (Fig. 4d). When changing the current density from 50 mA g^{-1} to 100 mA g^{-1}, 200 mA g^{-1}, 300 mA g^{-1} and 500 mA g^{-1}, the discharge capacities progressively decrease from 910 mA h g^{-1} to 753 mA h g^{-1}, 532 mA h g^{-1}, 364 mA h g^{-1} and 260 mA h g^{-1}, respectively. After the current density comes back to 200 mA g^{-1}, 100 mA g^{-1} and 50 mA g^{-1}, the average discharge capacities quickly resume, indicating an excellent cycling performance. Furthermore, we did a stability test of **NENU-601** at a current density of 500 mA g^{-1}. **NENU-601** exhibits a high reversible capacity (Fig. 4e) of 470 mA h g^{-1} after 200 cycles. Meanwhile, when comparing the capacity of the 200th cycle with the 2nd cycle, the capacity retention is 118.33%, profiting from pore activation. All of these results reveal the extraordinary performance of **NENU-601** for application in LIBs. A possible mechanism for the capacity contribution of **NENU-601** is shown in Fig. S9 and S10 (ESI†).

In summary, designing a strategy of choosing a suitable POM as a node and regulating the angle and length of mixed ligands is crucial to construct a ZPOMOF. In this work, by utilizing ε-{$Zn_4PMo_{12}O_{40}$} units as the POM node and 1,4-H_2bdc and Hbzt ligands as linkers we successfully synthesized the first ZPOMOF, **NENU-601**, with a framework in the ABW topological classification. As we expected, **NENU-601** exhibits high chemical and thermal stability and excellent performance for direct use in LIBs as an anode material. It is reliable for producing high capacities, a stable cycling performance and a restorable rate performance. A reversible capacity of 780 mA h g^{-1} was delivered after 200 cycles at a current density of 100 mA g^{-1}, indicating that POMOFs with a zeolite framework have great potential and wide application prospects in energy storage. What's more, our ZPOMOF structure enriches the variety of POMOFs, which also provides novel ideas for the structural design of MOFs or POMOFs.

This work was financially supported by the NSFC (No. 21371099 and 21471080), the Jiangsu Specially-Appointed Professor, the NSF of Jiangsu Province of China (No. BK20130043 and BK20141445), the Natural Science Research of Jiangsu Higher Education Institutions of China (No. 13KJB150021), the Priority Academic Program Development of Jiangsu Higher Education Institutions, and the Foundation of Jiangsu Collaborative Innovation Center of Biomedical Functional Materials.

Conflicts of interest

There are no conflicts to declare.

Notes and references

1 V. Van Speybroeck, K. Hemelsoet, L. Joos, M. Waroquier, R. G. Bell and C. R. A. Catlow, *Chem. Soc. Rev.*, 2015, **44**, 7044–7111.
2 A. Primo and H. Garcia, *Chem. Soc. Rev.*, 2014, **43**, 7548–7561.
3 Y. Li and J. Yu, *Chem. Rev.*, 2014, **114**, 7268–7316.
4 Y. Mu, N. Wang, Z. Sun, J. Wang, J. Li and J. Yu, *Chem. Sci.*, 2016, **7**, 3564–3568.
5 G. Feng, P. Cheng, W. Yan, M. Boronat, X. Li, J. H. Su, J. Wang, Y. Li, A. Corma and R. Xu, *Science*, 2016, **351**, 1188–1191.
6 Y. Li, J. Yu and R. Xu, *Angew. Chem., Int. Ed.*, 2013, **52**, 1673–1677.
7 J. Li, A. Corma and J. Yu, *Chem. Soc. Rev.*, 2015, **44**, 7112–7127.
8 T. Boyd, S. G. Mitchell, D. Gabb, D. L. Long, Y. F. Song and L. Cronin, *J. Am. Chem. Soc.*, 2017, **139**, 5930–5938.
9 D. Kim, X. Liu and M. S. Lah, *Inorg. Chem. Front.*, 2015, **2**, 336–360.
10 L. Wang, Y. Han, X. Feng, J. Zhou, P. Qi and B. Wang, *Coord. Chem. Rev.*, 2016, **307**, 361–381.
11 F. Zou, X. Hu, Z. Li, L. Qie, C. Hu, R. Zeng, Y. Jiang and Y. Huang, *Adv. Mater.*, 2014, **26**, 6622–6628.
12 L. Zhu, X. Q. Liu, H. L. Jiang and L. B. Sun, *Chem. Rev.*, 2017, **117**, 8129–8176.
13 J. Yu, L. H. Xie, J. R. Li, Y. Ma, J. M. Seminario and P. B. Balbuena, *Chem. Rev.*, 2017, **117**, 9674–9754.
14 Y. Cui, Y. Yue, G. Qian and B. Chen, *Chem. Rev.*, 2011, **112**, 1126–1162.
15 A. Schoedel, M. Li, D. Li, M. O'Keeffe and O. M. Yaghi, *Chem. Rev.*, 2016, **116**, 12466–12535.
16 W. Lu, Z. Wei, Z. Y. Gu, T. F. Liu, J. Park, J. Tian, M. Zhang, Q. Zhang and T. Gentle III, *Chem. Soc. Rev.*, 2014, **43**, 5561–5593.
17 X. C. Huang, Y. Y. Lin, J. P. Zhang and X. M. Chen, *Angew. Chem.*, 2006, **118**, 1587–1589.
18 Y. Q. Tian, C. X. Cai, X. M. Ren, C. Y. Duan, Y. Xu, S. Gao and X. Z. You, *Chem. – Eur. J.*, 2003, **9**, 5673–5685.
19 J. S. Qin, D. Y. Du, W. L. Li, J. P. Zhang, S. L. Li, Z. M. Su, X. L. Wang, Q. Xu, K. Z. Shao and Y. Q. Lan, *Chem. Sci.*, 2012, **3**, 2114–2118.
20 Y. Y. Wang, M. Zhang, S. L. Li, S. R. Zhang, W. Xie, J. S. Qin, Z. M. Su and Y. Q. Lan, *Chem. Commun.*, 2017, **53**, 5204–5207.
21 S. Li, H. Ma, H. Pang, L. Zhang, Z. Zhang and H. Lin, *Inorg. Chem. Commun.*, 2014, **44**, 15–19.
22 L. Zhang, B. Shan, H. Yang, D. Wu, R. Zhu, J. Nie and R. Cao, *RSC Adv.*, 2015, **5**, 23556–23562.
23 D. Y. Du, J. S. Qin, S. L. Li, Z. M. Su and Y. Q. Lan, *Chem. Soc. Rev.*, 2014, **43**, 4615–4632.
24 Z. X. Chen, H. Y. Yang, M. L. Deng, Y. Ling, L. H. Weng and Y. M. Zhou, *Dalton Trans.*, 2012, **41**, 4079–4083.
25 M. Y. Li, F. Wang, Z. G. Gu and J. Zhang, *RSC Adv.*, 2017, **7**, 4872–4875.
26 L. M. Rodriguez-Albelo, A. R. Ruiz-Salvador, A. Sampieri, D. W. Lewis, A. Gómez, B. Nohra, P. Mialane, J. Marrot, F. Sécheresse and C. Mellot-Draznieks, *J. Am. Chem. Soc.*, 2009, **131**, 16078–16087.
27 J. S. Qin, D. Y. Du, W. Guan, X. J. Bo, Y. F. Li, L. P. Guo, Z. M. Su, Y. Y. Wang, Y. Q. Lan and H. C. Zhou, *J. Am. Chem. Soc.*, 2015, **137**, 7169–7177.
28 L. M. Rodriguez-Albelo, A. R. Ruiz-Salvador, D. W. Lewis, A. Gómez, P. Mialane, J. Marrot, A. Dolbecq, A. Sampieri and C. Mellot-Draznieks, *Phys. Chem. Chem. Phys.*, 2010, **12**, 8632–8639.
29 G. Rousseau, L. M. Rodriguez-Albelo, W. Salomon, P. Mialane, J. R. M. Marrot, F. Doungmene, I. L. M. Mbomekallé, P. de Oliveira and A. Dolbecq, *Cryst. Growth Des.*, 2014, **15**, 449–456.
30 Q. Huang, T. Wei, M. Zhang, L. Z. Dong, A. Zhang, S. L. Li, W. J. Liu, J. Liu and Y. Q. Lan, *J. Mater. Chem. A*, 2017, **5**, 8477–8483.
31 T. Wei, M. Zhang, P. Wu, Y. J. Tang, S. L. Li, F. C. Shen, X. L. Wang, X. P. Zhou and Y. Q. Lan, *Nano Energy*, 2017, **34**, 205–214.
32 S. Wang, Q. Wang, P. Shao, Y. Han, X. Gao, L. Ma, S. Yuan, X. Ma, J. Zhou and X. Feng, *J. Am. Chem. Soc.*, 2017, **139**, 4258–4261.
33 T. Yuan, Y. Jiang, W. Sun, B. Xiang, Y. Li, M. Yan, B. Xu and S. Dou, *Adv. Funct. Mater.*, 2016, **26**, 2198–2206.